Journal of Biomechanics 130 (2022) 110888

Contents lists available at ScienceDirect

Journal of Biomechanics

journal homepage: www.elsevier.com/locate/jbiomech

In vitro motions of the medial and lateral proximal sesamoid bones under mid-stance load conditions are consistent with racehorse fracture configurations

Sarah K. Shaffer [a,*], Kassidy Shelly [b], Tanya C. Garcia [b], Monika A. Samol [c], Ashley E. Hill [c], David P. Fyhrie [d,e], Susan M. Stover [b]

[a] Department of Mechanical & Aerospace Engineering, University of California, Davis, United States
[b] Department of Surgical and Radiological Sciences, School of Veterinary Medicine, University of California, Davis, United States
[c] California Animal Health and Food Safety Laboratory System, University of California, Davis, Davis, CA, United States
[d] Department of Biomedical Engineering, University of California, Davis, United States
[e] Department of Orthopaedic Surgery, School of Medicine, University of California, Davis, United States

ARTICLE INFO

Keywords:
Racehorses
Kinematics
Bone Fracture

ABSTRACT

Proximal sesamoid bone (PSB) fractures in racehorses are likely fatigue fractures that occur due to repetitive loads and stress remodeling. The loading circumstances that may induce damage in the PSBs are not well understood. The goal of this study was to determine in three-dimensions, PSB motions relative to the opposing metacarpal condyle during simulated mid-stance loads. Seven equine cadaveric forelimbs were axially loaded in a material testing system to simulate standing and mid-stance walk, trot, and gallop load conditions (1.8–10.5 kN). Joint angles were determined by tracking the positions of bone-fixed kinematic markers. Internal-external rotation, abduction–adduction, and flexion–extension of each PSB relative to the third metacarpal condyle were compared between loads and between PSBs using an ANOVA with Tukey-Kramer post hoc tests for pairwise comparisons. The medial PSB rotated externally and the lateral PSB apex abducted during limb loading. Medial PSB external rotation was significantly greater at the gallop load condition than at the walk or trot load conditions. The medial and lateral PSB motions observed in this study are consistent with location of fatigue damage and fracture configurations frequently seen in medial and lateral PSBs from Thoroughbred racehorses. Specifically, medial PSB external rotation is consistent with the development of an abaxial subchondral medial PSB lesion that is reported in association with medial PSB transverse fracture and lateral PSB abduction is consistent with axial longitudinal fracture of the lateral PSB.

1. Introduction

Proximal sesamoid bone (PSB) fracture is a leading cause of death for Thoroughbred racehorses (Johnson et al., 1994; Sun et al., 2019; Wylie et al., 2017). Catastrophic PSB fracture is typically biaxial, meaning both the medial and lateral PSBs fracture. Biaxially fractured PSBs typically have different fracture configurations (Anthenill et al., 2006; Stover, 2013). Medial PSBs fracture transversely through the midbody to basilar portions of the bone, while the lateral PSBs fracture obliquely or transversely through the midbody to basilar portion of the bone or longitudinally along the axial border (Fig. 1; Anthenill et al., 2006). In California Thoroughbred racehorses, transverse midbody medial PSB fracture coupled with lateral PSB axial longitudinal fracture or intersesamoidean ligament rupture (Fig. 1) accounts for 5.4% of fatal fetlock injuries; a majority (73%) of these occur with a lateral condylar fracture of the third metacarpal bone (MC3; Hill, 2021). Biaxial PSB fractures (excluding axial longitudinal lateral PSB fractures) account for 50.4% of fatal fetlock injuries, generally in this fracture configuration the medial PSB fractures transversely and the lateral PSB fractures obliquely. Most biaxial PSB fractures (92%) occur without involvement of the MC3 (Hill, 2021).

Evidence indicates that PSB fractures are repetitive, overuse injuries (Riggs, 2002; Stover, 2003). Subchondral bone lesions found in the medial PSB have been associated with transverse fracture (Fig. 1;

* Corresponding author.
E-mail address: skshaffer@ucdavis.edu (S.K. Shaffer).

https://doi.org/10.1016/j.jbiomech.2021.110888
Accepted 12 October 2021
Available online 27 November 2021

Anthenill et al., 2010; Shaffer et al., 2020b; Stover, 2013). Lesion characteristics are consistent with damage induced bone remodeling (Ayodele et al., 2020; Shaffer et al., 2020b, 2020a), suggesting that there is a biomechanical mechanism that repeatedly causes high subchondral bone stress at the lesion location prior to fracture. While lateral PSB axial longitudinal fractures have not been thoroughly investigated, the consistency of this fracture configuration also implies a potential biomechanical etiology.

The medial and lateral PSBs are embedded in the suspensory apparatus of the distal portion of the forelimb and support the metacarpophalangeal joint (MCPJ) during locomotion. Four bones constitute the MCPJ: the third metacarpal bone (MC3), medial PSB, lateral PSB, and proximal phalanx (P1). The MC3 has two distinct portions of its distal articular surface, one congruent with the PSBs and the other with the P1; the PSBs do not articulate with P1. Previously, the authors reported that PSBs extend beyond their congruent articular surface on the MC3 at racing-speed loads and that some external rotation of the PSBs occurs during limb loading (Shaffer et al., 2021a,b). However, the full nature of PSB motion was not determined.

The purpose of the present study was to assess the full three-dimensional movements of the PSBs relative to the MC3 during in vitro limb loading. Our goal is to determine if PSB motions are consistent with the reported location of fatigue damage and fracture configurations for the medial and lateral PSBs. We hypothesize that during simulation of mid-stance racing-speed gallop, the PSBs would rotate externally and the lateral PSB would abduct relative to the long-axis of the MC3.

2. Materials and methods

Cadaveric forelimbs were loaded in vitro to simulate walk, trot, and gallop mid-stance loads. MCPJ joint angles were determined from bone-fixed kinematic markers, calibrated to a reference frame.

2.1. Sample selection

Seven cadaveric unilateral forelimbs (5 left, 2 right) were a convenience sample from horses euthanized for reasons unrelated to forelimb pathology (4 mares, 3 geldings; 4 Thoroughbreds in race training (2–4 years; 380–493 kg), 1 Paint (5 years; weight unknown), 1 Quarter Horse (14 years; 537.5 kg), and 1 Warmblood (21 years; 570 kg)). Owners provided informed consent for unrestricted or research use of cadavers. Limbs were harvested during clinical necropsy, wrapped in saline soaked towels, and stored frozen (-20°C; up to 16 months) until thawed at room temperature (21°C) for 24 h prior to biomechanical testing.

Forelimbs were transected at mid-radius to retain the accessory ligaments of the superficial and deep digital flexor tendons and the fetlock stay apparatus. Horseshoes, when present, were removed prior to biomechanical testing.

2.2. Limb instrumentation

The proximal end of each forelimb was fixed in a cylinder with polymethylmethacrylate (Coe Tray Plastic, GC America, Alsip IL) while

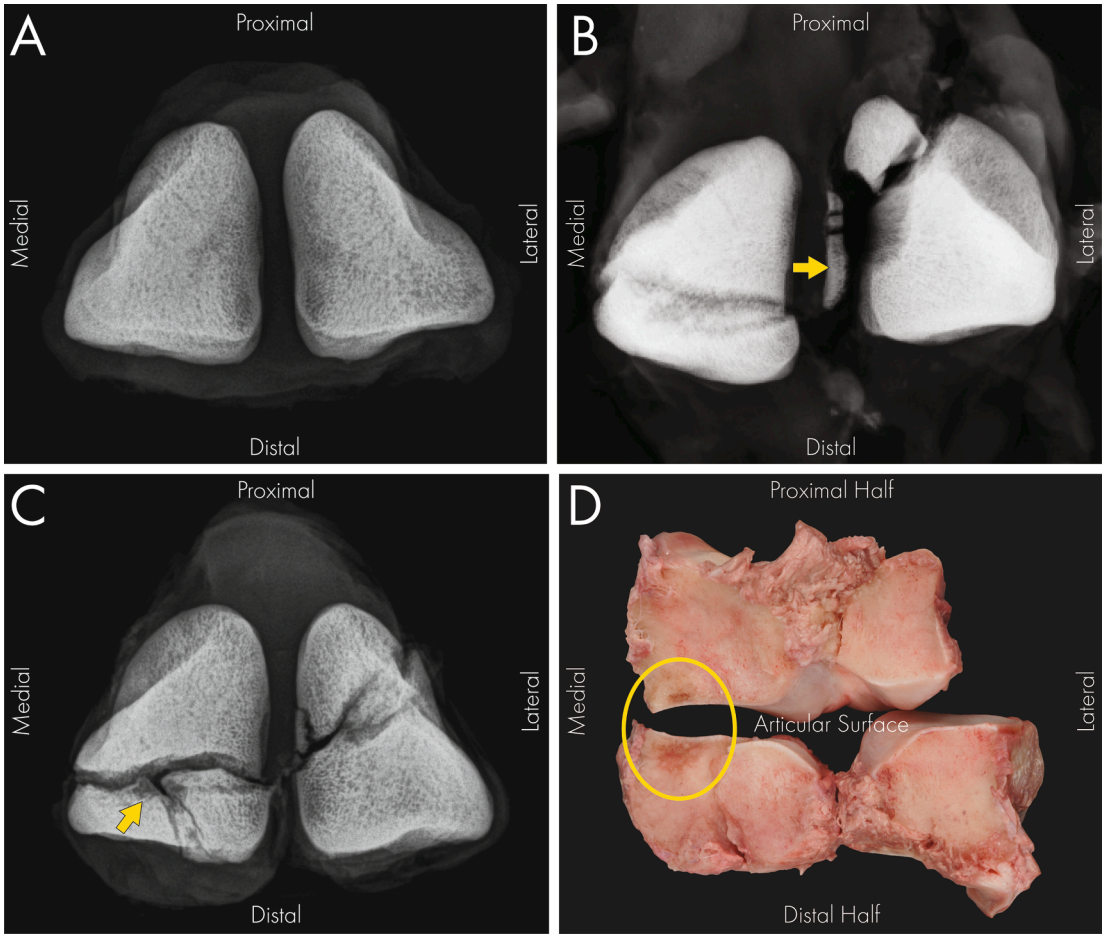

Fig. 1. Dorsopalmar radiographic projection of intact Proximal Sesamoid Bones (PSBs; Panel A) and examples of common bilateral PSB fracture configurations in Panels B and C. Panel B) Medial mid-body PSB fracture with a lateral axial longitudinal PSB fracture; the yellow arrow shows where the intersesamoidean ligament avulsed lateral PSB fragments. Panel C) Medial mid-body PSB fracture with a lateral oblique apical fracture; the yellow arrow indicates the site of a subchondral bone lesion illustrated on the fracture faces (yellow circle) of the medial PSB in Panel D. (For interpretation of the references to colour in this figure legend, the reader is referred to the web version of this article.)

the limb was in a standing position (Shaffer et al., 2021a,b; Singer et al., 2013). Fixation pins (3.2 mm diameter; Smooth Fixation Pin, IMEX Veterinary Inc.) were inserted perpendicularly to the median plane of the MC3 and P1 (Fig. 2). In each PSB, one 5 mm long 3.2 mm diameter fixation pin (Duraface, IMEX Veterinary Inc.) was inserted palmarly, abaxial to the flexor tendons and palmar to the insertion of the suspensory ligament (Fig. 2).

Spherical markers covered by reflective tape (3 M Scotchlite 3710) were attached to these pins to track bone movements. Single spherical markers (9.53 mm diameter) were attached to the MC3 pins. Orthogonal kinematic marker sets (30 mm height/width/depth with 8 mm diameter spheres, 3D printed Onyx, Mark2 Markforged) were attached to the PSB pins (Fig. 3). Planar kinematic marker sets were attached to the P1 pins (30 mm height/width with 8 mm diameter spheres, 3D printed, Onyx, Mark2 Markforged; Fig. 2).

2.3. Biomechanical testing

In vitro biomechanical testing was performed with a servohydraulic material testing system equipped with an axial–torsional load transducer (Model 809 and Model 662.10A-08; MTS Systems Corp., Minneapolis, MN). The radius was secured to the material testing system via the polymethylmethacrylate cylinder. The hoof was placed on a linear bearing translation table attached to the material testing system actuator, so that the radius and MC3 were parallel to the load axis under ~ 700 N compression (Fig. 2; Shaffer et al., 2021a,b; Singer et al., 2013). During loading the hoof moved dorsally and the MC3 remained parallel to the load axis (Shaffer et al., 2021a,b; Singer et al., 2013). Dorsopalmar radiographs were taken to convert marker positions to bone reference frames (Next DR, Sound Carlsbad, CA; HF100/30 +, MinXray, Inc., Northbrook, IL; 70 kVp, 2.0 mAs). The limb was preconditioned for 200 cycles of 700–1,800 N compression at 0.25 Hz, then loaded once from 700 to 10,500 N, and unloaded prior to testing. Limbs were tested from 700 to 10,500 N under displacement control at 5 mm/s while marker positions were recorded at 60 Hz with 2 high-speed video cameras (S-PRI, AOS Technologies AB, Dattwil Switzerland) in a calibrated field of view (Motion Analysis Calibration Cube, CF-20, Santa Rosa, CA).

2.4. Data reduction

Radiographic distances from kinematic markers to bone longitudinal axes were used to transform MC3 and P1 marker positions to bone-fixed virtual markers along the proximo-distal axes of MC3 and P1 (Singer et al., 2013); these defined the bone-fixed coordinate systems for MC3 and P1 in kinematic software (Motus 10.0, Contemplas GmbH, Kempten Germany). Kinematic triads were used to define the bone fixed axes for the PSBs. For all bones, the Z-axis was positive proximally and Y-axis positive dorsally, and the X-axis completed a right-handed coordinate system (positive medially in left limb, laterally in right limb; Fig. 3; Grood and Suntay, 1983). A joint coordinate system was then established for the MC3-P1, MC3-medial PSB, and MC3-lateral PSB articulations of the MCPJ in the kinematic analysis program. Flexion-extension angles occur about the MC3′s X-axis, internal-external rotation occurs about the P1′s Z-axis for the MC3-P1 or the PSB's Z-axis for MC3-PSB rotation, and abduction–adduction angles about the joint coordinate system's mutual perpendicular axis (Grood and Suntay, 1983). Custom equations, based on Grood (1983), were applied in kinematic analysis software to determine MC3-P1 angles (defined as movement of the P1 relative to MC3; Fig. 2) and PSB-MC3 joint angles (defined as movement of PSBs relative to MC3; Fig. 3).

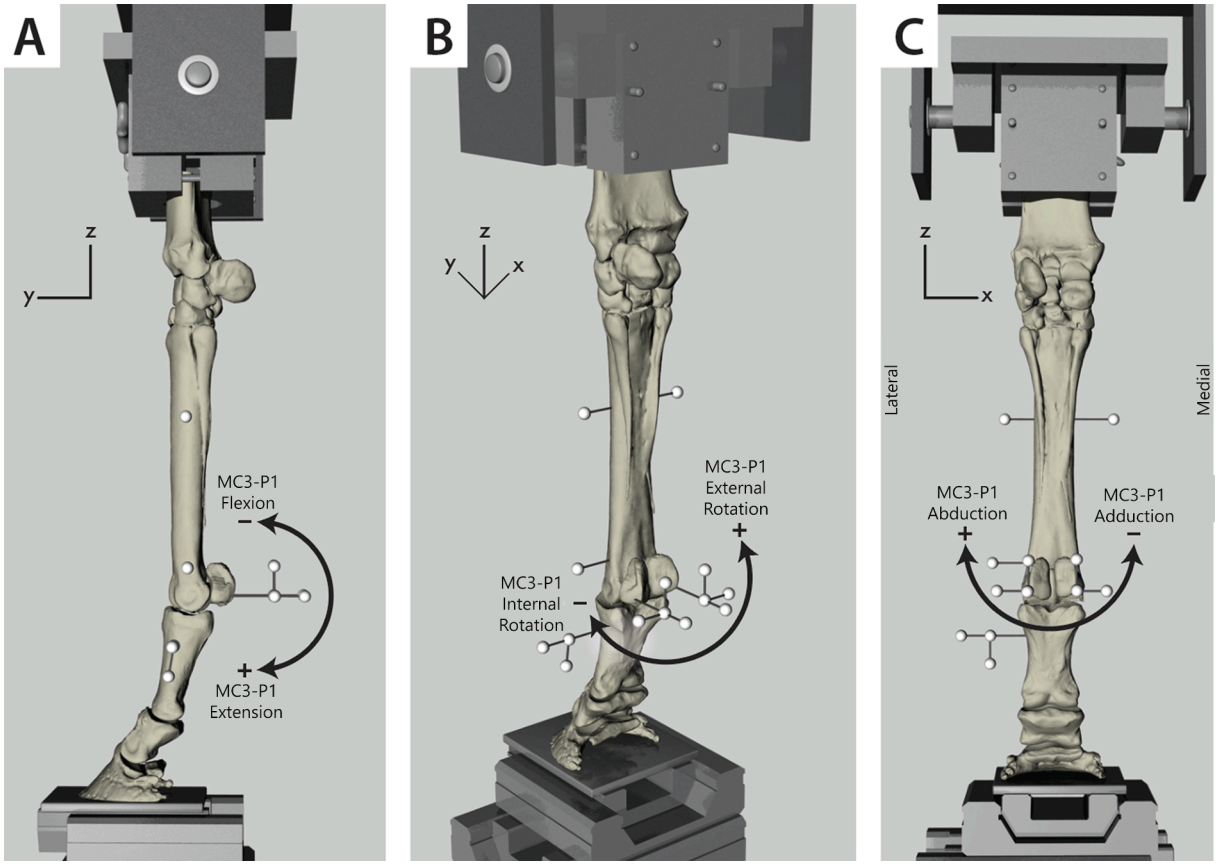

Fig. 2. Lateral (A), lateropalmar (B), and palmar (C) views illustrating instrumentation of a left forelimb in the material testing system showing MC3-P1 sign conventions for the flexion–extension, internal-external rotation, and abduction–adduction joint angles. The upper left corner of each panel indicates the positive direction of the coordinate axes (X, Y, Z) used for all bones. Note that all supporting soft tissues were maintained during tests, but are not shown in figures.

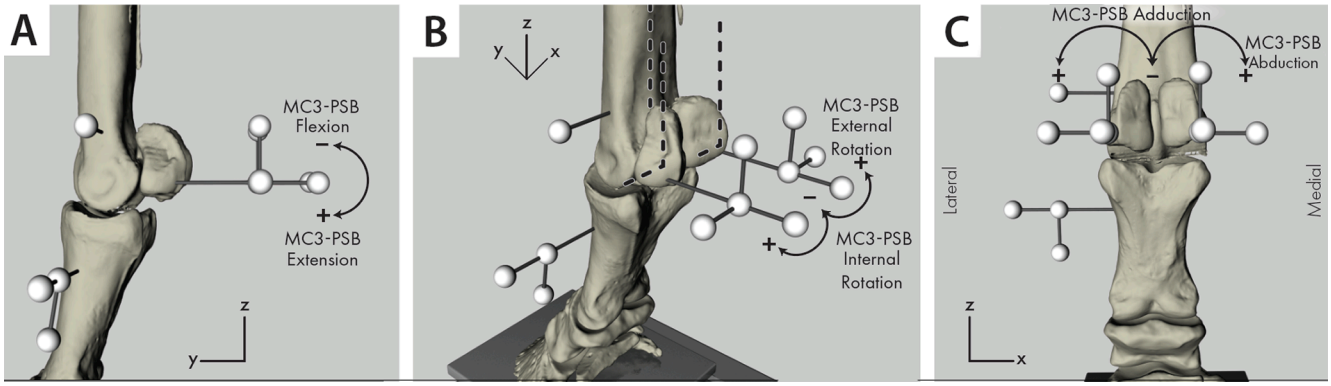

Fig. 3. Lateral (A), lateropalmar (B), and palmar (C) views illustrating instrumentation and sign conventions for the MC3-PSB flexion–extension, internal-external rotation, and abduction–adduction joint angles are shown on a left forelimb. The positive direction of the coordinate axes (X, Y, Z) are illustrated for all bones. Note that all supporting soft tissues were maintained during tests, but are not shown in figures.

The MC3-P1 flexion–extension angle is the palmar angle between P1 and MC3; it increases with MCPJ extension (Fig. 2; Singer et al., 2013). The MC3-P1 internal-external rotation angle increases with external rotation of P1 relative to MC3 (i.e., the dorsal aspect of P1 moves laterally relative to MC3; Fig. 2); MC3-P1 abduction–adduction angle increases with abduction (i.e., rotation of the proximal end of MC3 or distal end of P1 away from the body midline; Fig. 2). MC3-PSB angles were determined individually for the medial and lateral PSB. For all MC3-PSB angles, the flexion–extension angle increases as the PSB moves distally around the MC3 condyle during MCPJ extension, internal-external rotation angle increases with external rotation of the PSB relative to the midline of the MC3 (e.g. abaxial aspect of the PSB would move dorsally relative to the axial aspect of the PSB, or the axial aspect of the PSB would move palmarly relative to the abaxial aspect of the PSB), and abduction–adduction angle increases as the apex of the PSB moves away from the midline of the MC3 (Fig. 3).

Angle data were filtered with a low-pass filter (5 Hz cutoff; MATLAB R2020a, The MathWorks Inc., Natick, MA) followed with a robust linear regression smoothing filter (sampling window 45 units; MATLAB 2020a).

2.5. Data analysis

Metacarpophalangeal joint angles (MC3-P1, MC3-medial PSB, and MC3-lateral PSB) at Stand (1800 N) and mid-stance Walk (3600 N), Trot (4500 N), and Gallop (10500 N) load conditions were extracted from angle-load curves. Loads are consistent with in vivo peak vertical ground reaction forces during mid-stance and with previous in vitro studies (Brama et al., 2001; Schryver et al., 1978; Setterbo et al., 2009; Shaffer et al., 2021a,b; Singer et al., 2013; Swanstrom et al., 2005). The gallop load condition is consistent with estimates from simulation of 18 m/s gallop for a 500 kg horse (Swanstrom et al., 2005).

The effect of load condition (Walk, Trot, Gallop) and PSB side (Medial, Lateral) on the changes in MC3-PSB joint angles from the Stand load condition were assessed using ANOVA. The effects of load condition on MC3-P1 angle and on the change of MC3-P1 angle from Stand were also assessed using an ANOVA. Repeated measures within limbs were accounted for by incorporating horse as a random effect; Tukey-Kramer corrections were made for the post-hoc pairwise comparisons. A p-value ≤ 0.05 was statistically significant. Normality of model residuals were assessed via a Shapiro-Wilks score (W; $W > 0.90$ for all models). For analyses with non-normally distributed residuals, a ranked ANOVA was used. The effects of horse age, breed (Thoroughbred or non-Thoroughbred), limb side (left or right) and the load-limb side interaction were examined but were not significant.

The relationships between load and MC3-P1 and MC3-PSB joint angle differences from Stand sampled every 1050 N (10% of peak load) starting at 2100 N, were determined using linear regressions. Coefficient of determination (R^2) values are reported for statistically significant ($p \leq 0.05$) relationships. Partial Spearman correlation coefficients, controlling for horse, were determined for MC3-P1 flexion–extension and MC3-PSB joint angles; significant correlation coefficients (r; $p \leq 0.05$) are reported.

3. Results

Limb loading caused MCPJ extension and external rotation of P1 about MC3 (Table 1). The change in MC3-P1 extension from Stand increased linearly with load ($R^2 = 0.89$) and was significantly different among all load conditions (Table 1). The MC3-P1 extended 36° between the Stand and Gallop conditions. The change in MC3-P1 external rotation from Stand had a weak linear relationship with load ($R^2 = 0.31$) and 3.8° of MC3-P1 external rotation occurred between the Stand and Gallop conditions. The MC3-P1 did not experience statistically significant amounts of abduction or adduction.

Limb loading caused extension (distal motion) of both PSBs relative to the MC3. There were no significant differences in MC3-PSB flexion–extension angle between medial and lateral PSBs at any load condition. PSB extension changed 26° between Stand and Gallop; which was greater than the changes from Stand to Walk and Trot (Table 2). The change in PSB-MC3 extension from Stand increased linearly with load

Table 1
Least Square Mean ± Standard Error of MC3-P1 angles at Stand, Walk, Trot, and Gallop load conditions and the Change in MCPJ angles from the Stand load condition.

	Flexion (-)/Extension (+)		Internal (-)/External (+) Rotation		Adduction (-)/Abduction(+)	
	Angle†	Angle Change from Stand†	Angle§	Angle Change from Stand §	Angle§	Angle Change from Stand §
Stand	222.27 ± 2.24^{A}	NA	1.93 + 2.32^{A}	NA	4.98 + 1.79^{A}	NA
Walk	231.71 ± 2.24^{B}	9.44 ± 1.50^{A}	2.50 + 2.32^{A}	0.57 ± 0.94^{A}	4.84 + 1.79^{A}	−0.14 ± 0.82^{A}
Trot	236.82 ± 2.24^{C}	14.55 ± 1.50^{B}	3.04 + 2.32^{A}	1.11 ± 0.93^{A}	5.13 + 1.79^{A}	0.15 ± 1.15^{A}
Gallop	258.48 ± 2.24^{D}	36.21 ± 1.50^{C}	5.75 + 2.32^{B}	3.82 ± 3.83^{B}	5.49 + 1.79^{A}	0.51 ± 3.42^{A}

Note: MC3 (third metacarpal bone); P1 (proximal phalanx)
Significant effects: †ANOVA, § ranked ANOVA
^{A,B,C,D} : pairwise comparisons among load conditions; values within a column that do not share a superscript are statistically different at $p \leq 0.05$ with Tukey-Kramer adjustment

Table 2
Least Square Mean ± Standard Error of MC3-PSB angles from the Stand load condition for the Walk, Trot, and Gallop load conditions. Within a column, for each effect (separated by bold lines), values that share a superscript are not statistically different.

Load Condition	PSB Side	Flexion (-)/Extension (+) Angle Change from Stand †	Internal (-)/External (+) Rotation Angle Change from Stand †,‡,¶	Adduction (-)/Abduction(+) Angle Change from Stand ‡
Walk	.	$5.87 + 1.24^{A}$	$0.82 + 0.44^{A}$	$0.18 + 0.41^{A}$
Trot	.	$9.09 + 1.24^{B}$	$1.11 + 0.44^{A}$	$0.33 + 0.41^{A}$
Gallop	.	$26.02 + 1.24^{C}$	$3.67 + 0.44^{B}$	$0.98 + 0.41^{A}$
.	Lateral	$13.71 + 1.19^{\alpha}$	$1.04 + 0.38^{\alpha}$	$1.01 + 0.34^{\alpha}$
.	Medial	$13.61 + 1.19^{\alpha}$	$2.69 + 0.38^{\beta}$	$-0.01 + 0.34^{\beta}$
Walk	Lateral	$5.87 + 1.39^{1}$	$0.8 + 0.59^{1}$	$0.38 + 0.58^{1}$
Walk	Medial	$5.86 + 1.39^{1}$	$0.84 + 0.59^{1}$	$-0.02 + 0.58^{1}$
Trot	Lateral	$9.06 + 1.39^{1}$	$0.64 + 0.59^{1}$	$0.6 + 0.58^{1}$
Trot	Medial	$9.12 + 1.39^{1}$	$1.58 + 0.59^{1}$	$0.06 + 0.58^{1}$
Gallop	Lateral	$26.19 + 1.39^{2}$	$1.67 + 0.59^{1}$	$2.04 + 0.58^{1}$
Gallop	Medial	$25.84 + 1.39^{2}$	$5.67 + 0.59^{2}$	$-0.07 + 0.58^{1}$

Note: MC3 (third metacarpal bone), PSB (proximal sesamoid bone)
Significant ANOVA effects: † Load condition, ‡ PSB side, ¶ Load Condition and PSB Side interaction
^{A,B,C,D} : pairwise comparisons among load conditions, $p \leq 0.05$ with Tukey-Kramer adjustment
$^{\alpha,\beta}$: pairwise comparisons among PSB Side, $p \leq 0.05$ with Tukey-Kramer adjustment
^{1,2} : pairwise comparisons load condition and PSB side interaction, $p \leq 0.05$ with Tukey-Kramer adjustment

(Fig. 4A).

Both PSBs rotated externally as the limb was loaded; however, the medial PSB experienced more external rotation than the lateral PSB (Table 2; Fig. 4B). Between Stand and Gallop, the medial PSB externally rotated 5.7° and the lateral PSB externally rotated 1.7° (Table 2; Fig. 4B); the difference between Stand and Gallop was significant only for the medial PSB. The change in external rotation of the medial and lateral PSBs had strong and weak linear relationships with load, respectively (Fig. 4B).

The apex of the lateral PSB experienced significantly more abduction than the medial PSB; however, load condition did not have a significant effect on PSB abduction. Averaged over all load conditions, the abduction change from Stand was higher for the lateral PSB than medial PSB. The change in lateral PSB abduction from Stand had a weak linear relationship with load and the lateral PSB abducted 2° between the Stand and Gallop loads (Table 2; Fig. 4C). There was no similar significant relationship for the medial PSB.

The MC3-medial PSB external rotation increased with abduction of the MC3-lateral PSB (r = 0.52; Table 3). The MC3-medial PSB adduction increased as the MC3-lateral PSB externally rotated (r = -0.55) and abducted (r = -0.65). Additionally, lateral PSB external rotation increased with lateral PSB abduction (r = 0.55).

4. Discussion

The primary movement of both PSBs during axial limb loading is extension relative to MC3, which occurs as the PSBs wrap distodorsally around the MC3 condyle to support the limb during stance. The current study indicates that the medial and lateral PSBs have similar sagittal plane motion but differing non-sagittal plane motions during axial limb loading that are exaggerated at high-speed gallop loads. The medial PSB rotated externally more than the lateral PSB throughout loading and medial PSB external rotation was greatest for Gallop loads. The lateral PSB abducted more than the medial PSB during limb loading; however, abduction was not significantly different among load conditions.

Study results showing large amounts of flexion–extension compared to small out-of-plane rotations for MC3-P1, MC3-medial PSB, and MC3-lateral PSBs were expected since bone and soft tissue structures in the MCPJ confine its motion primarily to flexion–extension within the sagittal plane (Fig. 5). The sagittal ridge of the MC3 condyle interdigitates with both the sagittal groove on the proximal articular surface of P1 and the intersesamoidean ligament between the two PSBs, and in conjunction with the collateral ligaments, confines MCPJ motion to the sagittal plane. The suspensory apparatus (SA) supports the palmar

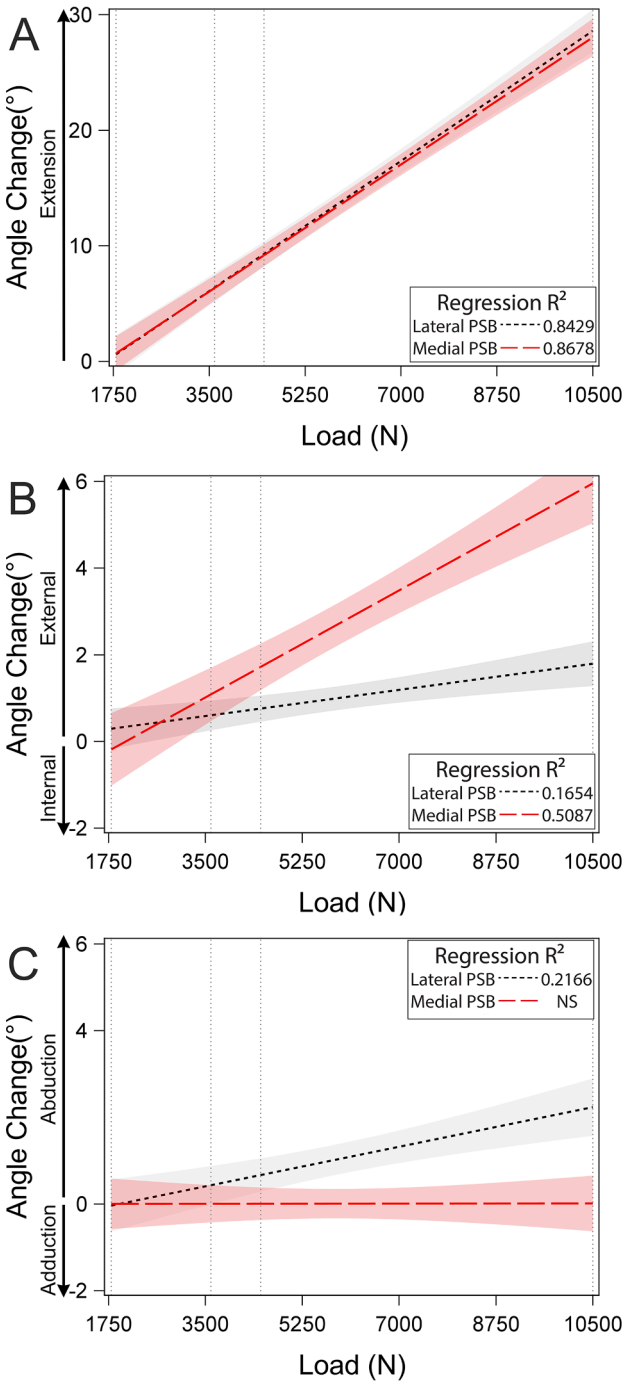

Fig. 4. Linear regressions and 95% confidence intervals for the change in medial MC3-PSB (red long-dashed line) and lateral MC3-PSB (black short-dashed line) angles from the Stand load condition for MC3-PSB flexion–extension angle (A), internal-external rotation angle (B), and abduction–adduction angle (C). Stand, Walk, Trot, and Gallop loads are indicated by vertical dashed lines. NS = non-significant. (For interpretation of the references to colour in this figure legend, the reader is referred to the web version of this article.)

Table 3
Partial Spearman correlation coefficients (r values) for the change of MC3-P1 angle and MC3-PSB angles from the Stance load condition for the Walk, Trot, and Gallop load conditions. Correlations are partial with respect to horse and all reported correlations are significant at $p \leq 0.05$.

		MC3-P1 Extension (+)	Medial PSB Joint Angle Change			Lateral PSB Joint Angle Change	
			Internal (-)/ External (+) Rotation	Adduction(-)/ Abduction(+)	Flexion (-)/ Extension(+)	Internal (-)/ External (+) Rotation	Adduction(-)/ Abduction(+)
Medial PSB Joint Angle Change	**Internal (-)/External (+) Rotation**	0.92	.	.	.	.	.
	Adduction(-)/ Abduction(+)	NS	NS	.	.	.	.
	Flexion (-)/ Extension (+)	0.98	0.91	NS	.	.	.
Lateral PSB Joint Angle Change	**Internal (-)/ External (+) Rotation**	NS	NS	−0.55	NS	.	.
	Adduction(-)/ Abduction(+)	0.64	0.52	−0.65	0.68	0.55	.
	Flexion (-)/ Extension (+)	0.98	0.92	NS	0.99	NS	0.71

Note: MC3 (third metacarpal bone); P1 (proximal phalanx), PSB (proximal sesamoid bone), NS (non-significant interaction; $p < 0.05$).

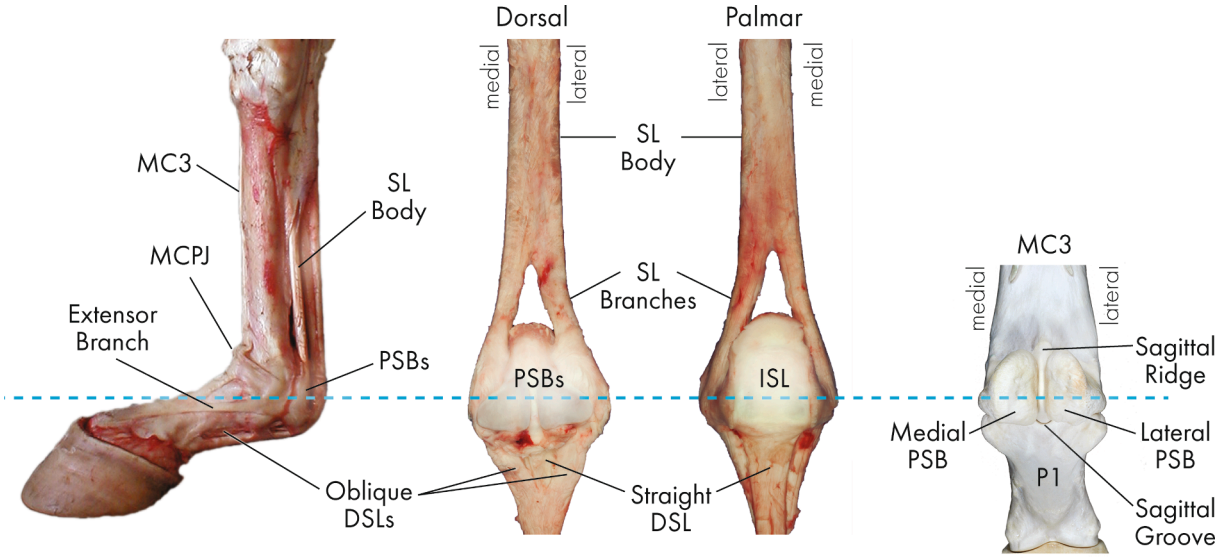

Fig. 5. Soft tissue structures and geometry of the bones of the metacarpophalangeal joint (MCPJ) help confine MCPJ motion to flexion–extension in the sagittal plane. Soft tissue components include the suspensory ligament (SL) and its medial, lateral, and extensor branches, the intersesamoidean ligament (ISL), and the distal sesamoidean ligaments (DSLs, distal ligaments of the proximal sesamoid bones (PSBs). Bones of the MCPJ include the third metacarpal bone (MC3), proximal phalanx (P1), and medial and lateral PSBs. The sagittal ridge of the MC3 condyle interdigitates with both the sagittal groove on the proximal articular surface of P1 and the ISL between the two PSBs.

aspect of the equine MCPJ, restricting excessive MCPJ extension. The SA consists of 3 structures in series, the suspensory ligament and its medial and lateral branches, the medial and lateral PSBs, and the distal ligaments of the PSBs (distal sesamoidean ligaments or DSLs). The SA originates from the proximal end of MC3 and inserts on P1 and the middle phalanx (P2). Within the SA, the suspensory ligament branches insert on the apices of the PSBs. The bases of the PSBs are bound tightly to P1 and P2 by four sets of DSLs, of which the straight and oblique DSLs are the most substantive. The PSBs are tightly bound to each other along their axial borders, on their respective sides of the sagittal ridge, by the intersesamoidean ligament.

Motion of the PSBs outside of the sagittal plane (i.e., outside of flexion–extension) may be related to PSB fracture configurations (Fig. 1). Within the same limb the medial and lateral PSBs often fracture in different configurations, and in this study, were shown to have different non-sagittal plane motions during limb loading. Medial PSBs often fracture transversely through the midbody to basilar portion of the bone (Anthenill et al., 2006) and a focal midbody abaxial subchondral bone lesion is believed to precede fracture and increase fracture risk (Fig. 1; Ayodele et al., 2020; Shaffer et al., 2020b). The observed external rotation of the medial PSB against the medial MC3 condyle could increase stresses on the abaxial portion of the PSBs articular surface and contribute to the formation of abaxial subchondral bone lesions. However, lateral PSB oblique, transverse, or axial longitudinal fracture often accompanies medial PSB transverse fracture (Fig. 1; Anthenill et al., 2006; Hill, 2021). In the current study, abduction of the apex of the lateral PSB was observed. PSB abduction may increase tension in the intersesamoidean ligament, which tightly binds the medial and lateral PSBs (Weaver et al., 1992). Increased stress along the axial border of the PSBs is consistent with axial longitudinal fracture and intersesamoidean ligament rupture.

Although the non-sagittal plane MC3-PSB rotations observed in this study were consistent with commonly observed pathologies in Thoroughbred racehorses, the cause of these movements is unknown. External rotation of P1 about MC3 as observed in this study and previously (Chateau, 2001; Merritt, 2010), may be responsible for the non-sagittal plane movement of the PSBs. External rotation of P1 relative to MC3 could facilitate external rotation of the medial PSB, since the

medial PSB is tightly bound to P1 via the medial collateral sesamoidean ligament (Fig. 6). If this interaction occurs, the higher MC3-P1 external rotations observed in vivo (Clayton et al., 2007) indicates that MC3-PSB external rotation is greater in live horses. External rotation of the medial PSB and constraint of the lateral PSB by the MC3 sagittal ridge may increase stress on the intersesamoidean ligament and axial border of the lateral PSB. External rotation of P1 relative to MC3 may increase stress on the base of the lateral PSB by the lateral oblique distal sesamoidean ligament (OSL) and contribute to abduction of the apex of the lateral PSB (Fig. 6). Lateral OSL lesions are more prevalent than medial OSL lesions in Thoroughbred racehorses, and lesions within the suspensory apparatus were associated with 4.6 times increased odds of having suffered a suspensory apparatus failure (e.g. PSB fracture, suspensory ligament rupture, or distal sesamoidean ligament rupture; Hill et al., 2016). Collectively, these factors could promote lateral PSB axial longitudinal fracture or intersesamoidean ligament rupture.

Horse- and training-specific factors may influence MC3-PSB rotations. Individual MCPJ conformation and shoeing may impact the direction of MC3-P1 internal-external rotation and abduction–adduction (Chateau et al., 2001; Clayton et al., 2007), so conformation may impact PSB-MC3 rotations. Additionally, in Thoroughbreds, medial PSBs are shorter and wider than lateral PSBs and the medial MC3 condyle tends to be larger than the lateral condyle (Alrtib et al., 2013; Anthenill et al., 2006; Beccati et al., 2014); the size differences combined with specific articular surface geometries may contribute to the amount of non-sagittal motion. However, geometries of PSB and MC3 articular surfaces are not known in enough detail to support or refute this idea. Finally, horseshoe (e.g., mediolateral geometry) and race-surface characteristics (e.g. uneven footing) affect forelimb kinetics and kinematics (Chateau et al., 2001; Harvey et al., 2012; Roepstorff et al., 1999), so may also affect MC3-PSB rotations. This study indicates that medial PSB external rotation and lateral PSB abduction increases with MC3-P1 extension; so, horses with conformation, horseshoes, or other characteristics that increase MC3-P1 extension may experience greater non-sagittal plane MC3-PSB rotations.

The MC3-P1 angles observed in this study were consistent with previous work (Butcher and Ashley-Ross, 2002; Chateau et al., 2001; Clayton et al., 2007; Setterbo et al., 2008; Singer et al., 2013). Mean MC3-P1 extension at Walk, Trot, and Gallop are consistent with in vivo studies (Butcher and Ashley-Ross, 2002; Setterbo et al., 2008; Singer et al., 2013). Mean MC3-P1 external rotation and abduction between Stand and Gallop is consistent with an in vitro study (Singer et al., 2013), but less than the external rotation and abduction observed in vivo (Clayton et al., 2007).

MC3-P1 abduction was not observed in the current or other in vitro studies that restricted mediolateral hoof movement and/or kept the hoof at a neutral position (Chateau, et. al., 2001; Singer, et. al., 2003). However, there is evidence that P1 abduction occurs in vivo during limb loading (18 ± 7°at trot, Clayton, et. al., 2007) and in vitro during asymmetric hoof placement (Chateau, et. al., 2001). MC3-P1 abduction would induce bending about the fetlock joint, increasing compression on the lateral side of the joint and tension on the medial side. This hypothesis is supported by higher density tissue observed in the lateral MC3 condyle, compared to the medial condyle (Riggs, et. al., 1999). Mediolateral bending during fetlock extension may also contribute to characteristic racehorse fetlock fracture patterns (Fig. 7). Transverse fracture is more common in the medial PSB (70%) than in the lateral PSB (30%, Anthenill, et. al., 2006) which is consistent with medial PSB failure under tension (Markel, 1992). Since bone is generally weaker in tension than compression, and lesions that predispose to fracture are common in the medial PSB (Shaffer, et. al., 2021), fetlock failure may be initiated by tension in the medial PSB. Oblique and axial longitudinal fractures are more common in the lateral PSB than the medial PSB (Anthenill, et. al., 2006), which is consistent with compression contributing to lateral PSB failure. Further, 73% of biaxial PSB fractures involving medial PSB fracture and lateral PSB axial longitudinal fracture or axial intersesamoidean ligament rupture also involve lateral MC3 condylar fracture (a complex fetlock breakdown). These complex fetlock breakdowns can similarly be attributed to excessive compressive loading of the lateral MC3 condyle. Variations in lateral PSB abduction may affect risk for complex breakdowns, by altering loading along the axial aspect of the lateral PSB. However, 92% of biaxial PSB fractures, involving medial PSB transverse and lateral PSB oblique fractures, are not associated with MC3 condylar fracture. Lateral compartment compression, due to MC3-P1 abduction, also offers a possible explanation for the higher prevalence of lateral MC3 condylar fractures (76–85%; Johnson, et. al. 1994; Zekas, et. al.,1999) compared to medial condylar fractures (8–15%), despite the larger geometry and surface area of the medial condyle (Dyce Anatomy; Alrtib, et. al., 2013). Speculating further, a common P1 fracture configuration originates in or near the sagittal groove and courses obliquely distally to exit the lateral cortex (Smith, et. al., 2014). This fracture configuration is consistent with P1 abduction and excessive compressive loading of the lateral aspect of the bone column. Importantly, in vitro evidence indicates

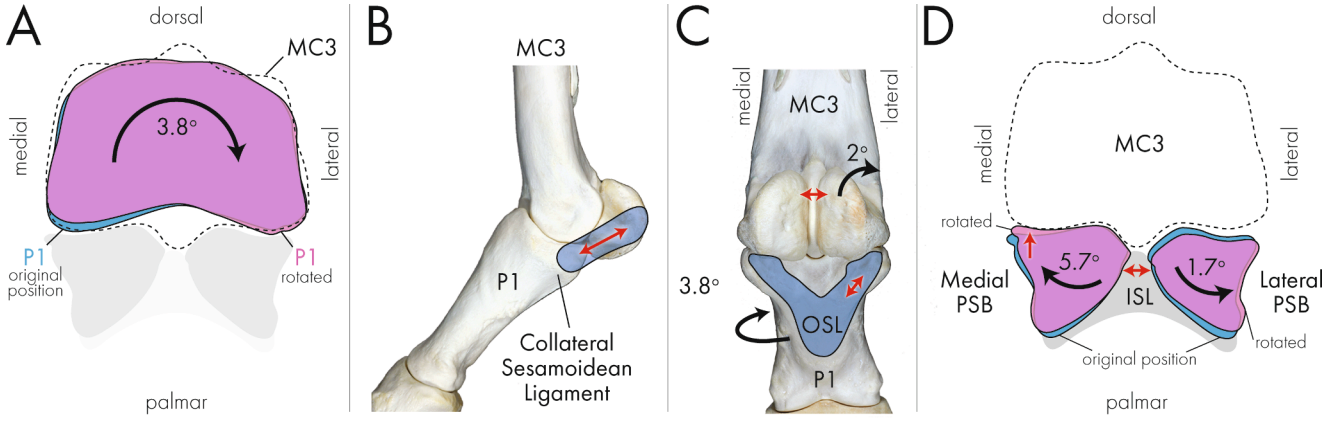

Fig. 6. Non-sagittal plane rotations of the proximal phalanx (P1) and the proximal sesamoid bones (PSBs) relative to the third metacarpal bone (MC3) and the potential interaction between these rotations and metacarpophalangeal joint ligaments at gallop equivalent load. External rotation of P1 about MC3 (Panel A) may increase tension in the medial collateral sesamoidean ligament (Panel B) and in the lateral branch of the lateral oblique sesamoidean ligament (OSL; Panel C). Increased tension in the medial collateral sesamoidean ligament may cause the observed external rotation of the medial PSB (Panel D) and increase contact between the medial PSB's abaxial surface and the MC3 condyle, promoting subchondral bone lesion formation. The non-sagittal plane PSB rotations likely increase tension in the intersesamoidean ligament (ISL; Panel D). Increased tension in the lateral OSL may cause the abduction and slight-internal rotation observed to occur on the lateral PSB; this may promote lateral PSB longitudinal fracture.

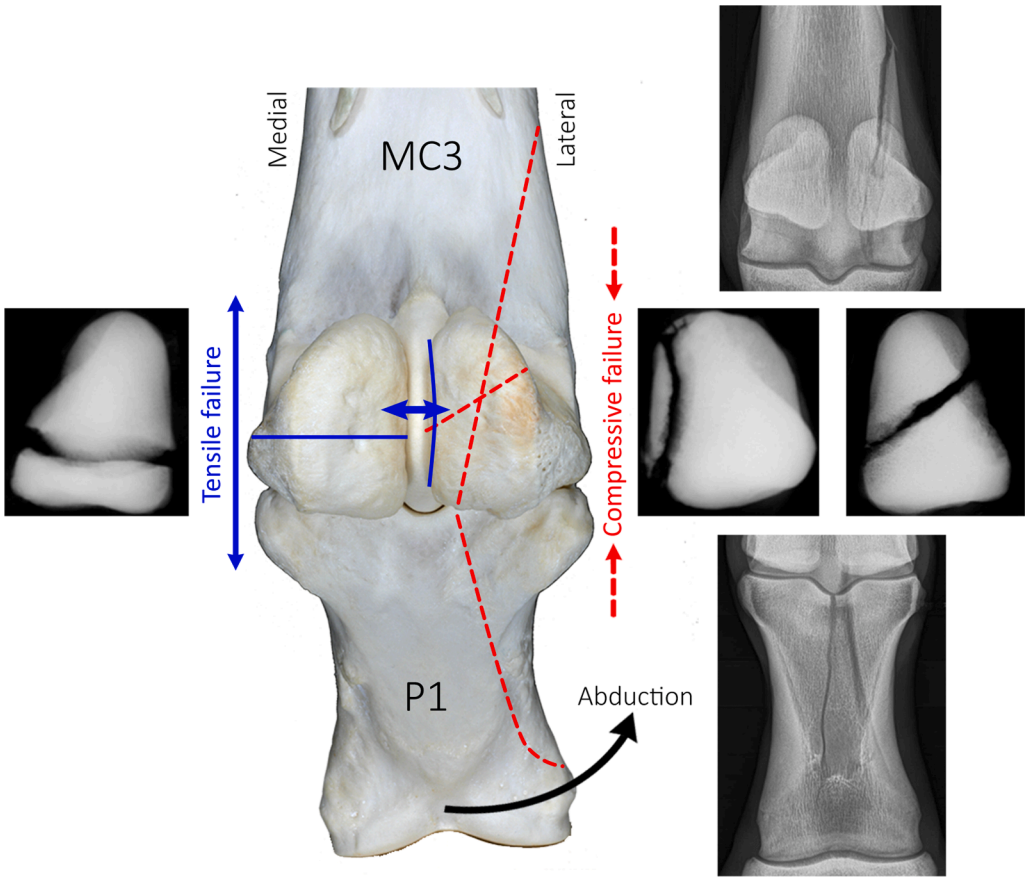

Fig. 7. Dorsopalmar radiographs illustrate characteristic fractures in the proximal sesamoid bones (PSBs), third metacarpal bone (MC3), and proximal phalanx (P1). Abduction of P1 relative to the MC3 during limb loading would induce bending about the fetlock joint with tension on the medial side of the joint and compression on the lateral side of the joint. The characteristic fracture patterns that occur in MC3, PSBs, and P1 are consistent with this loading condition. The medial PSB typically has a transverse fracture, consistent with tensile failure. The axial avulsion fracture of the lateral PSB is consistent with abduction of the apex of the lateral PSB and tension from the intersesamoidean ligament. The typical oblique fracture in the lateral PSB that commonly occurs with biaxial PSB fracture and the fractures in the lateral condyle of the MC3 and lateral oblique component common to some P1 fractures would be promoted by excessive compression on the lateral aspect of the fetlock.

MC3-P1 kinematics are influenced by hoof asymmetry (Chateau et. al., 2001; Chateau et. al., 2010, Denoix 1999), therefore hoof conformation, shoeing, and racetrack surface topography could affect risk or protection for fetlock failure.

The primary study limitation is that the study was performed in vitro instead of in vivo; however, in vivo PSB markers are impractical in live horses. In addition to presenting a significant welfare issue due to increased fracture risk, bone-fixed kinematic markers would be difficult to maintain during high-speed gallop as the fetlock can impact the ground. The slow, non-physiologic loading rates used in this study may have allowed for soft tissue stress relaxation during loading. However, the limbs were preconditioned and reported MC3-P1 extension angles are consistent with those from in vivo studies (Butcher and Ashley-Ross, 2002; Setterbo et al., 2008; Singer et al., 2013). Also, applied loads are consistent with the ranges for Stand (1.5–1.8 kN; Brama et al., 2001), Walk (3.9 – 3.5 kN; Schryver et al., 1978), Trot (4.4–8.1kN; Hjertén and Drevemo, 1994; Schryver et al., 1978; Setterbo et al., 2009) and Gallop (8.3–12.3kN; Kingsbury et al., 1978; Swanstrom et al., 2005) midstance (peak load) in previous studies estimated for a 500–600 kg horse. The sample size was adequate. Post hoc study power was > 0.9 for all significant study variables except for lateral PSB abduction using $\alpha = 0.05$; lateral PSB abduction had a power of 0.4. Although not all limbs were sourced from racehorses (4 Thoroughbred racehorses, 3 other breeds) and there was a wide age range for study horses (2 to 21 years), breed and age did not have statistically significant effects on study outcomes.

In summary, the medial and lateral PSBs experience different non-sagittal plane motions during biomechanical testing at loads consistent with a racing-speed gallop. External rotation of the medial PSB is consistent with midbody fractures commonly reported in medial PSBs and abduction of the lateral PSB is consistent with axial longitudinal fracture frequently seen in lateral PSBs.

Declaration of Competing Interest

The authors declare that they have no known competing financial interests or personal relationships that could have appeared to influence the work reported in this paper.

Acknowledgements

The authors thank Dr. Ellen Singer for her insightful comments on metacarpophalangeal anatomy and function. This work was supported by the University of California-Davis School of Veterinary Medicine Students Training in Advanced Research Program; Grayson Jockey Club Research Foundation, Center for Equine Health (with funds provided by the State of California satellite wagering fund and contributions from private donors) University of California-Davis, Maury Hull Fellowship, Louis R. Rowan Fellowship from the California Thoroughbred Foundation, and the Le Maitre Wild Oak Farm Endowment.

References

Alrtib, A.M., Philip, C.J., Abdunnabi, A.H., Davies, H.M.S., 2013. Morphometrical study of bony elements of the forelimb fetlock joints in horses. J. Vet. Med. Ser. C Anat. Histol. Embryol. 42 (1), 9–20. https://doi.org/10.1111/j.1439-0264.2012.01158.x.

Anthenill, L.A., Gardner, I.A., Pool, R.R., Garcia, T.C., Stover, S.M., 2010. Comparison of macrostructural and microstructural bone features in Thoroughbred racehorses with and without midbody fracture of the proximal sesamoid bone. Am. J. Vet. Res. 71 (7), 755–765. https://doi.org/10.2460/ajvr.71.7.755.

Anthenill, L.A., Stover, S.M., Gardner, I.A., Hill, A.E., Lee, C.M., Anderson, M.L., Barr, B. C., Read, D.H., Johnson, B.J., Woods, L.W., Daft, B.M., Kinde, H., Moore, J.D., Farman, C.A., Odani, J.S., Pesavento, P.A., Uzal, F.A., Case, J.T., Ardans, A.A., 2006. Association between findings on palmarodorsal radiographic images and detection of a fracture in the proximal sesamoid bones of forelimbs obtained from cadavers of racing Thoroughbreds. Am. J. Vet. Res. 67 (5), 858–868. https://doi.org/10.2460/ajvr.67.5.858.

Ayodele, B.A., Hitchens, P.L., Wong, A.S.M., Mackie, E.J., Whitton, R.C., 2021. Microstructural properties of the proximal sesamoid bones of Thoroughbred

racehorses in training. Equine Vet. J. 53 (6), 1169–1177. https://doi.org/10.1111/evj.v53.610.1111/evj.13394.
Beccati, F., Gialletti, R., Giontella, A., Davanzo, S., Di Meo, A., Pepe, M., 2014. Morphologic radiographic study of the proximal sesamoid bones of the forelimb in thoroughbred racehorses in training. J. Vet. Med. Ser. C Anat. Histol. Embryol. 43 (5), 403–407. https://doi.org/10.1111/ahe.2014.43.issue-510.1111/ahe.12075.
Brama, P.A.J., Karssenberg, D., Barnveld, A., Weeren, P.R., 2001. Contact areas and pressure distribution on the proximal articular surface of the proximal phalanx under sagittal plane loading. Equine Vet. J. 33 (1), 26–32. https://doi.org/10.2746/042516401776767377.
Butcher, M.T., Ashley-Ross, M.A., 2002. Fetlock joint kinematics differ with age in thoroughbred racehorses. J. Biomech. 35 (5), 563–571. https://doi.org/10.1016/S0021-9290(01)00223-8.
Chateau, H., Degueurce, C., Jerbi, H., Crevier-Denoix, N., Pourcelot, P., Audigié, F., Pasqui-Boutard, V., Denoix, J.M., 2001. Normal three-dimensional behaviour of the metacarpophalangeal joint and the effect of uneven foot bearing. Equine Vet. J. Suppl. 33, 84–88. https://doi.org/10.1111/j.2042-3306.2001.tb05366.x.
Chateau, H., Degueurce, C., Denoix, J.M., 2010. Three-dimensional kinematics of the distal forelimb in horses trotting on a treadmill and effects of elevation of heel and toe. Equine Vet J. 38, 164–169.
Clayton, H.M., Sha, D., Stick, J., Elvin, N., 2007. 3D Kinematics of the equine metacarpophalangeal joint at walk and trot. Vet. Comp. Orthop. Traumatol. 02 (02), 86–91. https://doi.org/10.1160/VCOT-07-01-0011.
Denoix, J.M., 1999. Functional Analtomy of the Equine Interphalangeal Joints. AAEP Proc. 45, 174–177.
Dyce, Sack and Wensing's Textbook of Veterinary Anatomy - E-Book. Saunders, 2017. Print.
Grood, E.S., Suntay, W.J., 1983. A joint coordinate system for the clinical description of three-dimensional motions: Application to the knee. J. Biomech. Eng. 105, 136–144. https://doi.org/10.1115/1.3138397.
Harvey, A.M., Williams, S.B., Singer, E.R., 2012. The effect of lateral heel studs on the kinematics of the equine digit while cantering on grass. Vet. J. 192 (2), 217–221. https://doi.org/10.1016/j.tvjl.2011.06.003.
Hill, A.E., 2021. Unpublished Data.
Hill, A.E., Gardner, I.A., Carpenter, T.E., Lee, C.M., Hitchens, P.L., Stover, S.M., 2016. Prevalence, location and symmetry of noncatastrophic ligamentous suspensory apparatus lesions in California Thoroughbred racehorses, and association of these lesions with catastrophic injuries. Equine Vet. J. 48 (1), 27–32. https://doi.org/10.1111/evj.12367.
Hjertén, G., Drevemo, S., 1994. Semi-quantitative analysis of hoof-strike in the horse. J. Biomech. 27 (8), 997–1004. https://doi.org/10.1016/0021-9290(94)90216-X.
Johnson, B.J., Stover, S.M., Daft, B.M., Kinde, H., Read, D.H., Barr, B.C., Anderson, M., Moore, J., Woods, L., Stoltz, J., Blanchard, P., 1994. Causes of death in racehorses over a 2 year period. Equine Vet. J. 26, 327–330. https://doi.org/10.1111/j.2042-3306.1994.tb04395.x.
Kingsbury, H.B.B., Quddus, M.A., Rooney, J.R., Geary, J.E., 1978. A laboratory system for production of flexion rates and forces in the forelimb of the horse. Am. J. Vet. Res. 39, 365–369.
Markel MD. Fracture Biology and Mechanics. In: Equine Surgery, JA Auer Editor. WB Saunders Co, Philadelphia, 1992 Pgs 798-807.
Merritt, J.S., Pandy, M.G., Brown, N.A.T., Burvill, C.R., Kawcak, C.E., McIlwraith, C.W., Davies, H.M.S., 2010. Mechanical loading of the distal end of the third metacarpal bone in horses during walking and trotting. Am. J. Vet. Res. 71 (5), 508–514. https://doi.org/10.2460/ajvr.71.5.508.
Riggs, C.M., Whitehouse, G.H., Boyde, A., 1999. Structural variation of the distal condyles of the third metacarpal and third metatarsal bones in the horse. Equine Vet. J. 31, 130–139. https://doi.org/10.1111/j.2042-3306.1999.tb03806.x.
Riggs, C.M., 2002. Fractures - A preventable hazard of racing thoroughbreds? Vet. J. 163 (1), 19–29. https://doi.org/10.1053/tvjl.2001.0610.
Roepstorff, L., Johnston, C., Drevemo, S., 1999. The effect of shoeing on kinetics and kinematics during the stance phase. Equine Exerc. Physiol. 5, 279–285.
Schryver, H.F., Bartel, D.L., Langrana, N., Lowe, J.E., 1978. Locomotion in the horse: kinematics and external and internal forces in the normal equine digit in the walk and trot. Am. J. Vet. Res. 39, 1728–1733.
Setterbo, J., Garcia, T., Campbell, I., Kim, S., Hubbard, M., Stover, S., 2008. In: The Engineering of Sport 7. Springer Paris, Paris, pp. 437–446. https://doi.org/10.1007/978-2-287-99056-4_54.
Setterbo, J.J., Garcia, T.C., Campbell, I.P., Reese, J.L., Morgan, J.M., Kim, S.Y., Hubbard, M., Stover, S.M., 2009. Hoof accelerations and ground reaction forces of Thoroughbred racehorses measured on dirt, synthetic, and turf track surfaces. Am. J. Vet. Res. 70 (10), 1220–1229. https://doi.org/10.2460/ajvr.70.10.1220.
Shaffer, S.K., Sachs, N., Garcia, T.C., Fyhrie, D.P., Stover, S.M., 2021a. In vitro assessment of the motion of equine proximal sesamoid bones relative to the third metacarpal bone under physiologic midstance loads. Am. J. Vet. Res. 82 (3), 198–206. https://doi.org/10.2460/ajvr.82.3.198.
Shaffer, S.K., Stover, S.M., Fyhrie, D.P., 2020a. Morphological Changes in Proximal Sesamoid Bones from Racehorses as a Model for Overuse Joint Injuries, in: ORS 2020 Annual Meeting. p. Paper No. 2312.
Shaffer, S.K., To, C., Garcia, T.C., Fyhrie, D.P., Uzal, F.A., Stover, S.M., 2021b. Subchondral focal osteopenia associated with proximal sesamoid bone fracture in Thoroughbred racehorses. Equine Vet. J. 53 (2), 294–305. https://doi.org/10.1111/evj.v53.210.1111/evj.13291.
Singer, E., Garcia, T., Stover, S., 2013. How do metacarpophalangeal joint extension, collateromotion and axial rotation influence dorsal surface strains of the equine proximal phalanx at different loads in vitro? J. Biomech. 46 (4), 738–744. https://doi.org/10.1016/j.jbiomech.2012.11.028.
Smith, M.R.W., Wright, I.M., 2014. Radiographic configuration and healing of 121 fractures of the proximal phalanx in 120 Thoroughbred racehorses (2007–2011). Equine Vet. J. 46 (1), 81–87. https://doi.org/10.1111/evj.12094.
Stover, S.M., 2013. Diagnostic Workup of Upper-Limb Stress Fractures and Proximal Sesamoid Bone Stress Remodeling, in: AAEP Proceedings; In-Depth: Racing-Related Lameness. pp. 427–435.
Stover, S.M., 2003. The Epidemiology of Thoroughbred Racehorse Injuries. Clin. Tech. Equine Pract. 2 (4), 312–322. https://doi.org/10.1053/j.ctep.2004.04.003.
Sun, T.C., Riggs, C.M., Cogger, N., Wright, J., Al-Alawneh, J.I., 2019. Noncatastrophic and catastrophic fractures in racing Thoroughbreds at the Hong Kong Jockey Club. Equine Vet. J. 51 (1), 77–82. https://doi.org/10.1111/evj.2019.51.issue-110.1111/evj.12953.
Swanstrom, M.D., Zarucco, L., Hubbard, M., Stover, S.M., Hawkins, D.A., 2005. Musculoskeletal Modeling and Dynamic Simulation of the Thoroughbred Equine Forelimb During Stance Phase of the Gallop. J. Biomech. Eng. 127, 318–328. https://doi.org/10.1115/1.1865196.
Weaver, J.C.B., Stover, S.M., O'Brien, T.R., 1992. Radiographic anatomy of soft tissue attachments in the equine metacarpophalangeal and proximal phalangeal region. Equine Vet. J. 24, 310–315. https://doi.org/10.1111/j.2042-3306.1992.tb02842.x.
Wylie, C.E., McManus, P., McDonald, C., Jorgensen, S., McGreevy, P., 2017. Thoroughbred fatality and associated jockey falls and injuries in races in New South Wales and the Australian Capital Territory, Australia: 2009–2014. Vet. J. 227, 1–7. https://doi.org/10.1016/j.tvjl.2017.06.008.
Zekas, L.J., Bramlage, L.R., Embertson, R.M., Hance, S.R., 1999. Characterisation of the type and location of fractures of the third metacarpal/metatarsal condyles in 135 horses in central Kentucky (1986–1994). Equine Vet. J. 31, 304–308. https://doi.org/10.1111/j.2042-3306.1999.tb03821.x.